



# Construction of Ultrastable porous carbons materials derived from organic/inorganic double decker silsesquioxane (DDSQ) hybrid as a high-performance electrode for supercapacitor

Cheng-Yu Chen<sup>a</sup>, Mohamed Gamal Mohamed<sup>a,b</sup>, Wei-Cheng Chen<sup>a</sup>, Shiao-Wei Kuo<sup>a,c,\*</sup>

<sup>a</sup> Department of Materials and Optoelectronic Science, Center for Functional Polymers and Supramolecular Materials, National Sun Yat-Sen University, Kaohsiung 80424, Taiwan

<sup>b</sup> Chemistry Department, Faculty of Science, Assiut University, Assiut 71515, Egypt

<sup>c</sup> Department of Medicinal and Applied Chemistry, Kaohsiung Medical University, Kaohsiung 807, Taiwan

## ARTICLE INFO

### Keywords:

DDSQ  
Organic/inorganic hybrid  
Thermal property  
And supercapacitor

## ABSTRACT

Three different types of organic/inorganic hybrids are synthesized through the hydrosilylation of the double-decker silsesquioxane (DDSQ) with divinylbenzene (DVB), 3,13-divinyl double-decker silsesquioxane (DV-DDSQ) and cubic octavinylsilsesquioxane (OVS) individually to form DVB-DDSQ, DVDDSQ-DDSQ, and OVS-DDSQ, was achieved through Fourier transform infrared (FTIR) and nuclear magnetic resonance (NMR) spectroscopy. Thermal stability using TGA analyses, it was observed that the OVS-DDSQ hybrid possesses the highest thermal stability with  $T_{d10}$  of 596 °C and a char yield of 82.2 wt% because of the improvement of the cross-linking structure and increased density within the OVS-DDSQ hybrid. Furthermore, after carbonization to increase the surface area of OVS-DDSQ to form a microporous carbon (C-OVS-DDSQ) hybrid framework, it displays electrochemical performance with specific capacitances of 146 F g<sup>-1</sup> at 0.5 A g<sup>-1</sup>, benefiting from its high surface area of 169 m<sup>2</sup> g<sup>-1</sup>, which facilitated efficient electron transfer and the presence of a lot of active sites on the electrode surface. Notably, the capacitance retention of the C-OVS-DDSQ hybrid remained excellent, reaching 98 % at 20 A g<sup>-1</sup> even after 5000 cycles, suggesting its remarkable stability.

## 1. Introduction

Polymer nanocomposites based on polyhedral oligomeric silsesquioxane (POSS) consist of the polymer matrix incorporating POSS units [1–8]. POSS is the nanoscale cage-like structure of a unique class composed of Si and O atoms, which could be functionalized with various organic groups such as epoxy, amine, acrylate, phenolic, and vinyl units [9–17]. The POSS units should be dispersed well into the polymer matrix in polymer POSS nanocomposites that could create hybrid properties featuring the advantage properties of both components. For example, the incorporation of POSS units into the polymers could provide several advantages including high thermal, mechanical, and barrier properties, as well as dimensional stability and flame retardancy because of its intrinsic inorganic silica cage structure [18–25]. In general, various approaches could be dispersed the POSS units in the polymer matrix including solution blending, melting blends, and in-situ polymerization from a covalent bond or the specific interactions such as hydrogen

bonding and dipole-dipole interaction between the POSS units and the polymer matrix [1,6,7,26–30]. Until now, the covalent bonding between polymer and POSS units is the most efficient approach to synthesizing polymer/POSS nanocomposites [1].

In our previous studies [1,6,7,31], we summarized the architectures of polymer/POSS nanocomposites with different topologies, which are strongly dependent on the functionality of the POSS units. Using a mono-functionalized POSS unit is the case where POSS units are positioned at the side chain or chain end of polymer/POSS nanocomposites [1,12,30]. In addition, the incorporation of multi-functionalized POSS units within the polymer matrix could form insoluble cross-linked structures and sometimes form porous frameworks [32–35]. Using bi-functionalized POSS units is another approach for the development of the main chain type of polymer/POSS nanocomposites such as polyimide, polybenzoxazine, polyurethane, and diblock copolymer system [1,31,36–39]. The double-decker silsesquioxane (DDSQ) derivatives are the well-known bi-functionalized POSS units that could be incorporated

\* Corresponding author.

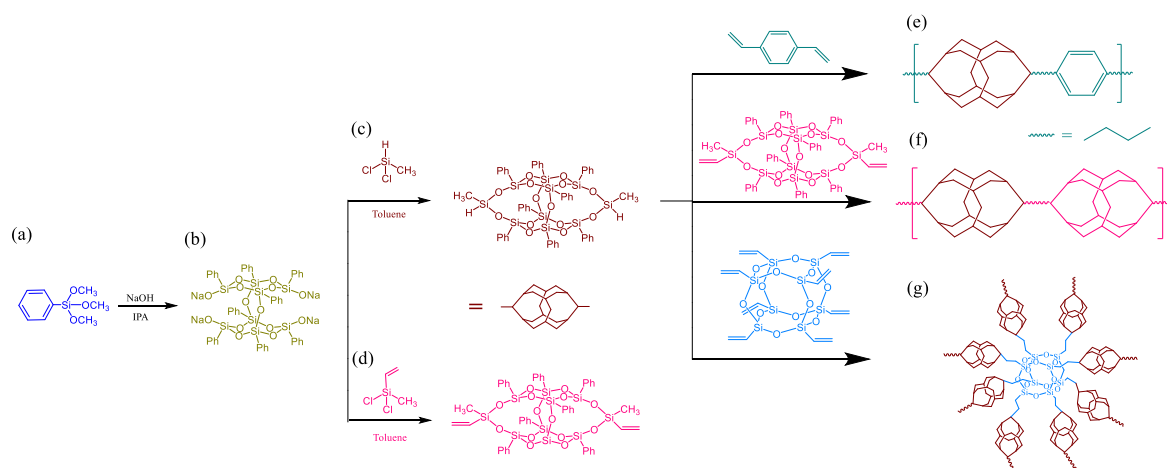
E-mail address: [kuosw@faculty.nsysu.edu.tw](mailto:kuosw@faculty.nsysu.edu.tw) (S.-W. Kuo).

<https://doi.org/10.1016/j.mtchem.2023.101773>

Received 19 June 2023; Received in revised form 14 September 2023; Accepted 12 October 2023

Available online 20 October 2023

2468-5194/© 2023 Elsevier Ltd. All rights reserved.



**Scheme 1.** Synthesis of DDSQ-based organic/inorganic hybrids from (a) phenyltrimethoxysilane, (b) DD-Na, (c) DDSQ, (d) DV-DDSQ, and then to form (e) DVB-DDSQ from DDSQ with DVB, (f) DVDDSQ-DDSQ from DDSQ with DV-DDSQ, and (g) OVS-DDSQ from DDSQ with OVS by hydrosilylation.

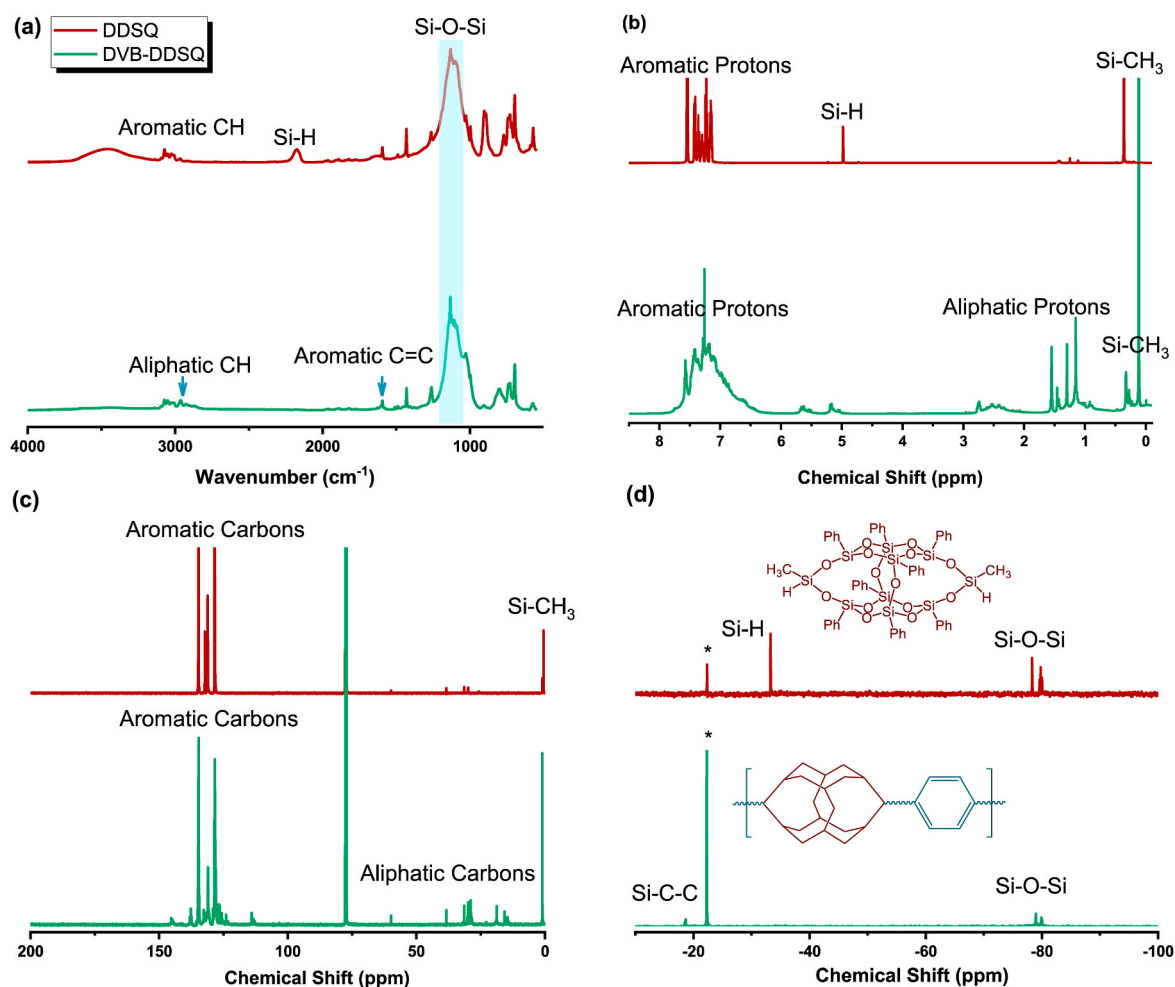


**Fig. 1.** The synthesis of DVB-DDSQ organic/inorganic hybrid from DDSQ with DVB and their corresponding (a) FTIR, (b)  $^1\text{H}$ , (c)  $^{13}\text{C}$ , and (d)  $^{29}\text{Si}$  NMR spectra.

into the main chain polymers with other bi-functionalized units and it also could form the crosslinking structures with multi-functionalized units [40–43]. As a result, the combination of DDSQ derivatives for the main chain polymer or crosslinking structure allows for the creation of hybrid materials, making them for various applications such as coating, composites, and electronic devices [40–43].

In recent years, environmental problems have attracted everyone's attention. The burning of a large amount of petroleum fuels has caused environmental problems and climate change [44]. Therefore, scientists have been actively searching for innovative and efficient renewable energy storage alternatives [44,45]. Electrochemical energy storage has become one of the most convenient options among various solutions.

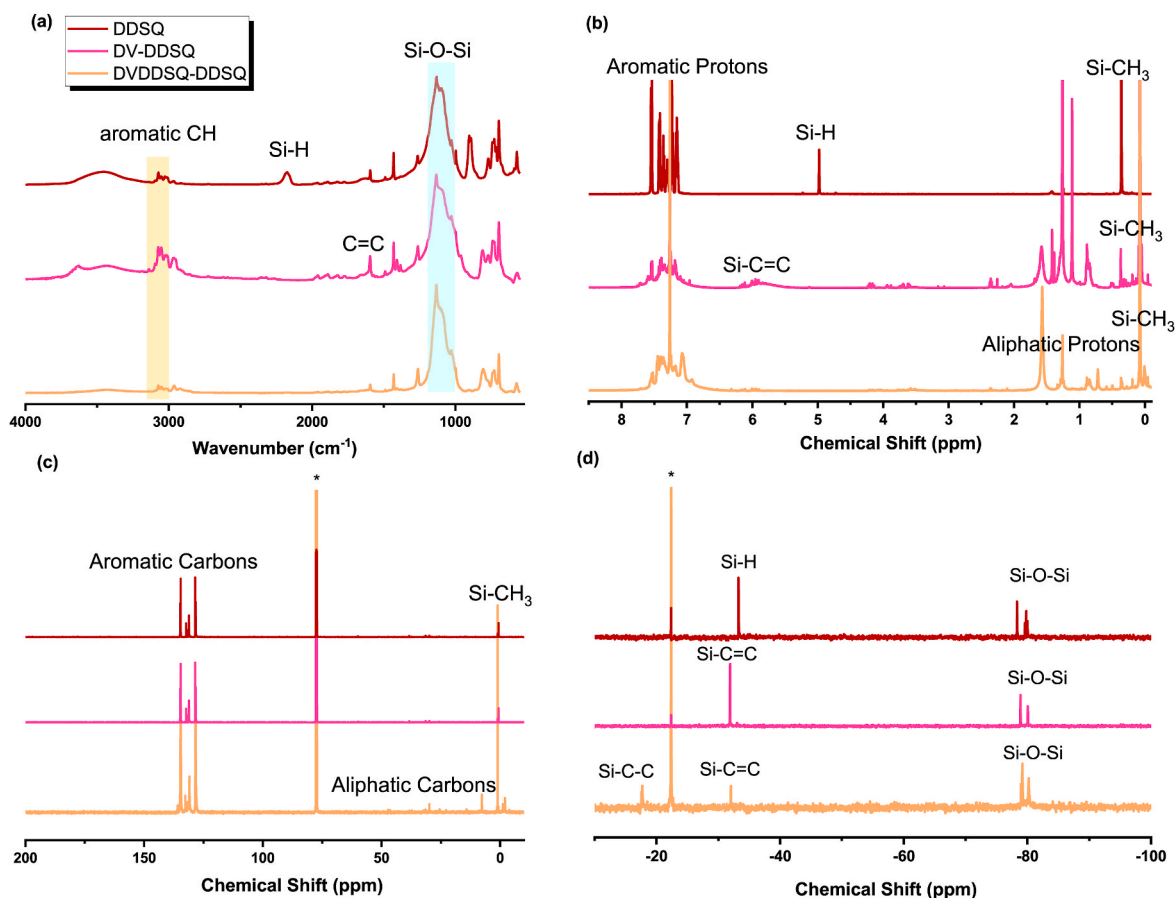


Fig. 2. The synthesis of DVDDSQ-DDSQ organic/inorganic hybrid from DDSQ with DV-DDSQ and their corresponding (a) FTIR, (b) <sup>1</sup>H, (c) <sup>13</sup>C, and (d) <sup>29</sup>Si NMR spectra.

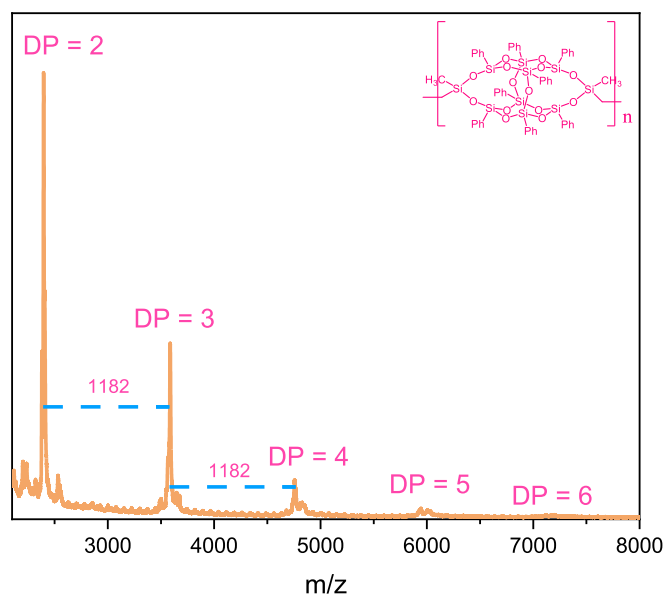


Fig. 3. MALDI-TOF mass spectrum of DVDDSQ-DDSQ hybrid.

These include rechargeable batteries, capacitors, and supercapacitors (SCs) [46–50], all of which have advantages and properties such as safety, reasonable capacity strength, fast charge/discharge rates, and long-cycle stability [51–55]. SCs, in particular, offers the added benefit of cheapness and long lifespan [56,57], making it show great promise

and progress in this field. According to the way of storing charge, supercapacitors can be divided into pseudocapacitors and electric double-layer capacitors (EDLC) [58–61]. Pseudocapacitors store energy by reversible redox reactions between electrolyte electrode materials and electrode materials [62,63]. On the other hand, EDLCs mainly store energy through physical procedures involving the adsorption/desorption of charged ions at the interface of the electrode-electrolyte [64, 65]. Therefore, EDLCs require a high surface area to achieve high capacitive performance [66,67]. Porous carbons have the advantages of high specific surface area, good electrical conductivity, and high stability [68–71]. Therefore, it has attracted more and more attention in energy applications [72–75]. In addition, many porous carbons have been developed, such as hollow carbon nanospheres [76], ordered/disordered mesoporous carbons [77], and ordered/disordered macroporous carbons [78]. But most of these porous carbons are prepared through templating methods [79] or high-temperature sintering [80]. Therefore, frameworks with higher thermal performance are required to be fabricated as precursors. Many studies have also confirmed that POSS is a porous polymer prepared as a building block, that possesses a high specific surface area and excellent thermal stability [81–88]. In this work, we synthesized three organic-inorganic hybrid materials with highly thermally stable and electrochemical responses incorporating two different types of POSS (DDSQ and OVS) through hydrosilylation. To understand the model reaction of DDSQ with OVS to form a hybrid framework of OVS-DDSQ, the other two different types of organic-inorganic hybrids were also synthesized through the hydrosilylation of the DDSQ with divinylbenzene (DVB) and DV-DDSQ to form main chain type of DVB-DDSQ and DVDDSQ-DDSQ hybrids, respectively. In addition, to enhance the electrochemical performance of OVS-DDSQ carbonization was employed to increase its surface area and

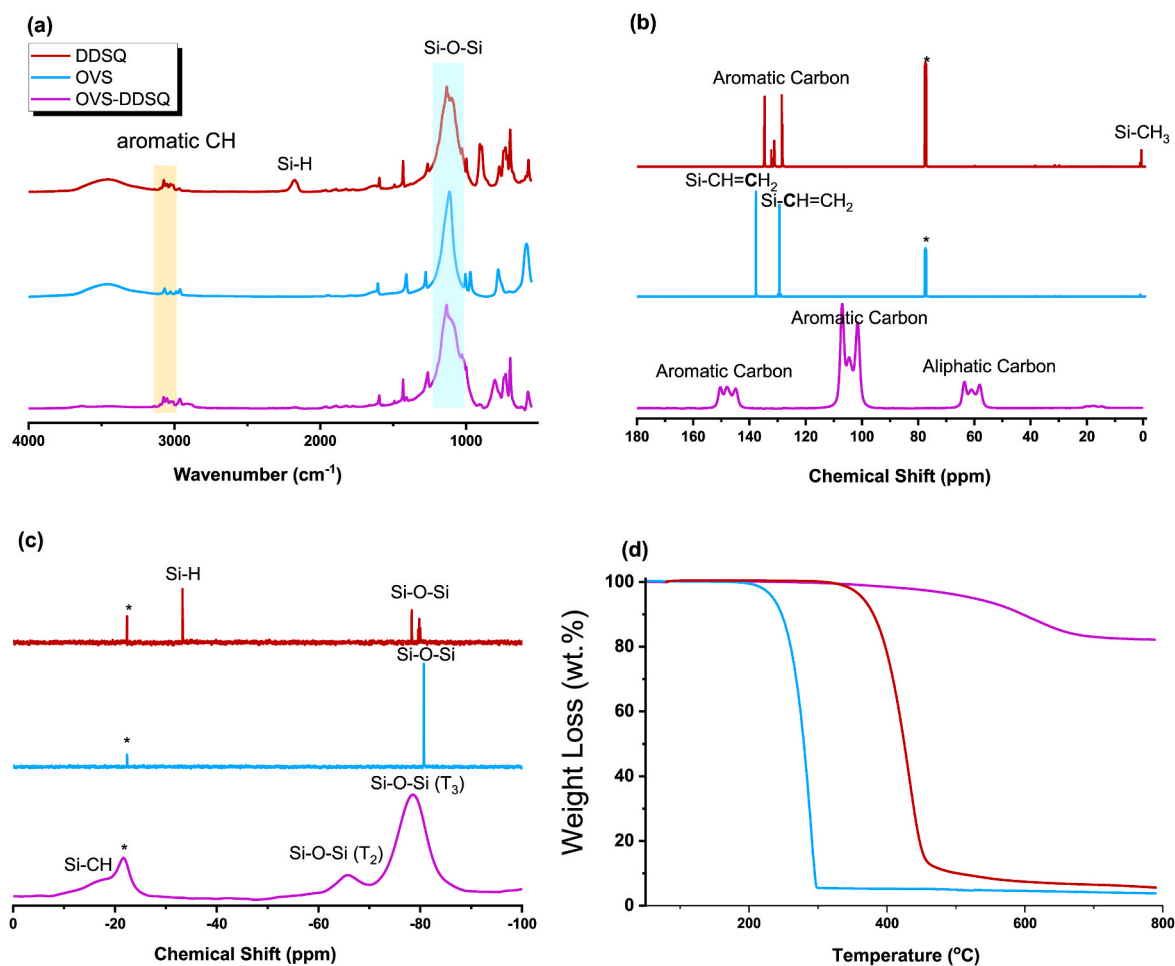


Fig. 4. The synthesis of OVS-DDSQ organic/inorganic hybrid framework from DDSQ with OVS and their corresponding (a) FTIR, (b)  $^{13}\text{C}$ , and (c)  $^{29}\text{Si}$  NMR spectra, and (d) TGA analyses.

it could provide high capacitance and capacitance retention. The detailed chemical structures, thermal properties, and electrochemical performance of these three DDSQ-derivative hybrids are also discussed in this study.

## 2. Experimental section

### 2.1. Materials

Divinylbenzene (DVB), phenyltrimethoxysilane, methyl dichlorosilane, vinylmethyl dichlorosilane, sodium hydroxide (NaOH), and platinum divinyltetramethyldisiloxane (Pt (dvs)) complex were acquired from Sigma-Aldrich. Octavinylsilsesquioxane (OVS) was purchased from Hybrid Plastic Company. Double-decker silsesquioxane-Na (DDNa) (Scheme 1(b)) and double-decker silsesquioxane (DDSQ) (Scheme 1(c)), and DV-DDSQ (Scheme 1(d)) were synthesized in our previous studies and the synthesis details were provided in supporting information [17,39].

### 2.2. Synthesis of DVB-DDSQ, DVDDSQ-DDSQ and OVS-DDSQ organic/inorganic hybrids

DDSQ (3 g, 2.6 mmol) with divinylbenzene (0.338 g, 2.6 mmol), DV-DDSQ (3.13 g, 2.6 mmol), or OV-POSS (0.41 g, 0.65 mmol) and toluene (40 mL) was stirred for 30 min with a reflux condenser in a flask. Frozen pumping was performed three times to remove any impurities. Afterward, Pt (dvs) (0.3 mL) was slowly added dropwise to the mixture,

which was subsequently heated under a nitrogen atmosphere at  $80\text{ }^{\circ}\text{C}$  for 72 h. Once the reaction was complete, the solid was filtered out of the mixture, and the filtrate was concentrated using vacuum distillation. The resulting residue was subjected to an oven treatment, producing in the formation of three different pale-yellow solids identified as DVB-DDSQ (2.7 g, yield: 80 %), DVDDSQ-DDSQ (5.5 g, yield: 89 %), and OVS-DDSQ (2.4 g, 70 %) as shown in Scheme 1(e), 1(f) and 1(g), respectively.

### 2.3. The preparation of porous carbon from OVS-DDSQ by carbonization

The OVS-DDSQ organic/inorganic hybrid was first placed in a tubular furnace from room temperature to  $600\text{ }^{\circ}\text{C}$  at a heating rate of  $2\text{ }^{\circ}\text{C min}^{-1}$  under  $\text{N}_2$  atmosphere. The mixture of OVS-DDSQ was stirred with aqueous KOH (OVS-DDSQ/KOH = 1/2) for 1 day at room temperature. Afterward, the water was removed, and the carbon powder prepared from the previous step was subjected to further carbonization at  $800\text{ }^{\circ}\text{C}$  in a tubular furnace for 2 h under  $\text{N}_2$  atmosphere. Finally, the porous carbon was washed by the deionized  $\text{H}_2\text{O}$  several times until the pH to 7 and put in the oven to obtain the black powder.

## 3. Results and discussion

### 3.1. Synthesis of DVB-DDSQ organic/inorganic hybrid

The synthesis of DVB-DDSQ organic/inorganic hybrid used DDSQ with DVB by hydrosilylation as shown in Scheme 1(d) as the model

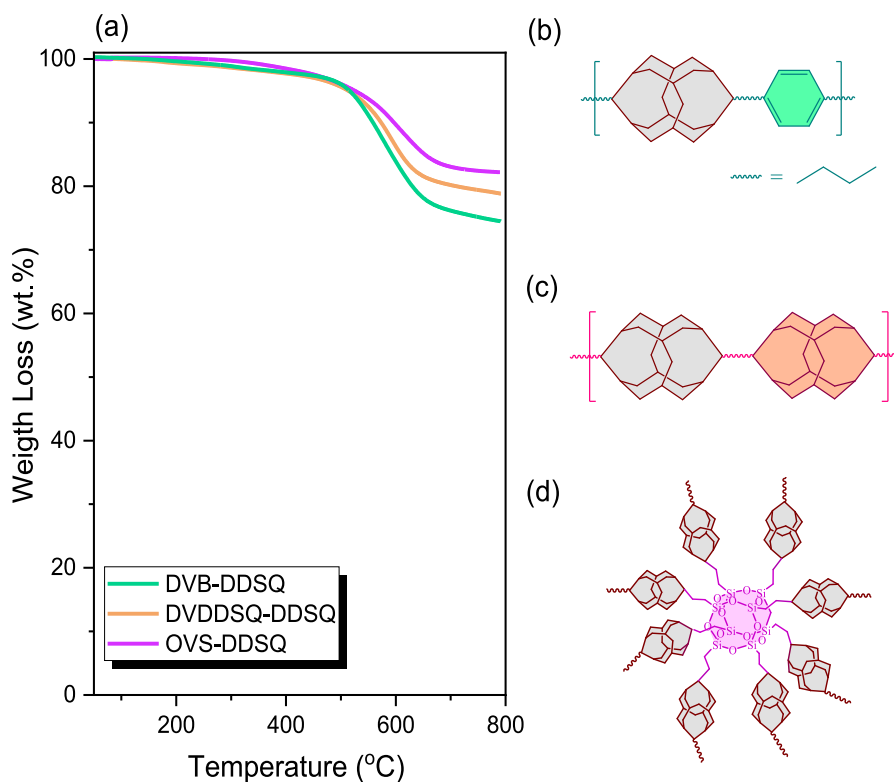


Fig. 5. (A) TGA thermal analyses and chemical structure of (b) DVB-DDSQ, (c) DVDDSQ-DDSQ, and (d) OVS-DDSQ hybrids.

reaction to prepare DVDDSQ-DDSQ and OVS-DDSQ. Fig. 1(a) displays their corresponding FTIR spectra, where the strong absorption at  $1264\text{ cm}^{-1}$  could be attributed to the Si–O–Si units, while the absorption at  $1264\text{ cm}^{-1}$  is due to the Si–CH<sub>3</sub> unit for pure DDSQ and DVB-DDSQ hybrid. Notably, the signal at  $2165\text{ cm}^{-1}$ , characteristic of pure DDSQ, disappeared after hydrosilylation with DVB to form a DVB-DDSQ hybrid. Additionally, the absorption at ca.  $0.2964\text{--}2810\text{ cm}^{-1}$ , representing aliphatic CH, and the aromatic C=C absorption at ca.  $1600\text{ cm}^{-1}$  from the DVB unit, increased after hydrosilylation, indicating the successful formation of the DVB-DDSQ hybrid. In addition, Fig. 1(b)–1(d) also provides <sup>1</sup>H, <sup>13</sup>C, and <sup>29</sup>Si NMR spectra of pure DDSQ and DVB-DDSQ hybrid. The signal of Si–H and Si–CH<sub>3</sub> units were observed at 4.68 ppm and 0.15 ppm, respectively, for pure DDSQ (Fig. 1(b)). After the hydrosilylation, the Si–H peak at 4.68 ppm disappeared and the aliphatic protons and carbons appeared at ca. 1–2.75 ppm in <sup>1</sup>H NMR (Fig. 1(b)) and ca. 14–38 ppm in <sup>13</sup>C NMR (Fig. 1(c)), respectively. Additionally, the aromatic protons and carbons from the DVB unit were also detected at ca. 6.64 ppm in <sup>1</sup>H NMR (Fig. 1(b)) and ca. 114 and ca. 145 ppm in <sup>13</sup>C NMR (Fig. 1(c)). Finally, Fig. 1(d) shows <sup>29</sup>Si NMR spectra, where the Si–O–Si unit was located at –78.16 and –79.88 ppm, representing the different environments of Si atoms within the DDSQ cage. Most importantly, the Si–H peak at –33.37 ppm, present in pure DDSQ, also disappeared after hydrosilylation to form a DVB-DDSQ hybrid. In its place, a new signal at 18.98 ppm corresponded to the new Si–CH<sub>2</sub> unit [86,87]. Furthermore, the DVB-DDSQ hybrid also possesses high thermal properties and stability, which exhibited a *T<sub>g</sub>* value of 260 °C (Fig. S1), *T<sub>d10</sub>* = 558 °C, char yield = 74.0 wt% that are significantly higher than pure DDSQ (*T<sub>d10</sub>* = 380 °C, char yield = 5.6 wt % in Fig. S2(a)). All results confirmed the successful synthesis of the DVB-DDSQ hybrid and its molecular weight also could be determined by using GPC analysis (*M<sub>n</sub>* = 17,900 g/mol, PDI = 1.38).

### 3.2. Synthesis of DVDDSQ-DDSQ organic/inorganic hybrid

DVDDSQ-DDSQ organic/inorganic hybrid was synthesized using hydrosilylation of DDSQ with DV-DDSQ as shown in Scheme 1(e) and their corresponding FTIR and <sup>1</sup>H spectra as shown in Fig. 2(a) and (b). Similarly, the Si–H peak at  $2165\text{ cm}^{-1}$  in FTIR spectra and 4.68 ppm signal in <sup>1</sup>H NMR of pure DDSQ disappeared. In addition, the vinyl protons of DV-DDSQ observed at 6.2 and 5.9 ppm also disappeared,<sup>88</sup> while the aliphatic carbons were still present at ca. 7–46 ppm in <sup>13</sup>C NMR spectra (Fig. 1(c)) after hydrosilylation to form DVDDSQ-DDSQ hybrid. Furthermore, Fig. 2(d) displays their corresponding <sup>29</sup>Si NMR spectra, where the Si–O–Si unit was almost located at a similar chemical shift at ca. –78.16 and –79.88 ppm for all three DDSQ derivatives. Firstly, the peak at –33.37 ppm due to the Si–H unit vanished and the new signal at –17.74 ppm was corresponding to a new Si–CH<sub>2</sub> unit. Secondly, the intensity of the Si–C=C unit of pure DV-DDSQ located at –31.87 ppm was decreased after hydrosilylation to form a DVDDSQ-DDSQ hybrid when compared with pure DV-DDSQ. The remaining Si–C=C unit of the DVDDSQ-DDSQ hybrid indicates the presence of the chain end group of DV-DDSQ derivative and thus we also used GPC to determine the molecular weight of DVDDSQ-DDSQ hybrid (*M<sub>n</sub>* = 7900 g/mol; PDI = 1.13), indicating the presence of ca. 6 DDSQ units in this main chain type of DVDDSQ-DDSQ hybrid.

In addition, we also used MALDI-TOF mass spectra to determine the chemical structure and molecular weight of this DVDDSQ-DDSQ hybrid as shown in Fig. 3. The mass difference between the signals at *m/z* 3585.08 (DP = 3) and *m/z* 4755.40 (DP = 4) was ca. 1170 g/mol, which is corresponding to the molecular weight of each DDSQ derivative, indicating a short methylene bridge between each DDSQ cage [89,90]. Most importantly, the higher degree of polymerization (DP) such as 5 and 6 are also observed for this DVDDSQ-DDSQ hybrid copolymer, further confirming the successful synthesis as supported by all characterizations used.

Furthermore, the DVDDSQ-DDSQ organic/inorganic hybrid also displayed remarkable thermal stability where the  $T_g$  value is 355 °C (Fig. S1),  $T_{d10}$  = 573 °C, char yield = 79.2 wt% (Fig. S2(b)). The higher concentration of DDSQ in DVDDSQ-DDSQ compared with DVB-DDSQ hybrid could possess higher thermal stability as expected. This is due to the incorporation of the more rigid inorganic DDSQ segment that replaces the only benzene ring in DVB-DDSQ which could increase thermal stability. Fig. S3 shows SEM and EXD analyses of DVB-DDSQ and DVDDSQ-DDSQ hybrids, indicating that no macro-phase separation and the DDSQ was dispersed well for both hybrids since the Si and O-mapping homogeneously on the surface. Furthermore, the weight percentage of Si and O atoms of the DVDDSQ-DDSQ hybrid is higher than the DVB-DDSQ hybrid as shown in Table S1 resulting in higher thermal stability as expected. Actually, the high thermal stability of DVDDSQ-DDSQ organic/inorganic hybrid makes it suitable for potential applications in thermal insulation or high-performance polymeric materials.

### 3.3. Synthesis of OVS-DDSQ organic/inorganic hybrid

To further increase the thermal properties of the DDSQ-based hybrid, we incorporated two types of POSS nanoparticles: octavinyl POSS (OVS) and DDSQ. This resulted in the formation of OVS-DDSQ organic/inorganic hybrid as the crosslinking structure through hydrosilylation as displayed in Scheme 1(g). Because of the crosslinking structure of the OVS-DDSQ hybrid, the chemical structure only could be determined by

solid-state FTIR,  $^{13}\text{C}$ , and  $^{29}\text{Si}$  NMR analyses as shown in Fig. 4(a)–4(c). Similar to previous hybrids, the Si–H peak at 2165  $\text{cm}^{-1}$  in FTIR spectra (Fig. 4(a)) and the peak at –33.37 ppm attributed to the Si–H unit in  $^{29}\text{Si}$  NMR spectra (Fig. 4(c)) were both disappeared. In addition, the vinyl carbons of OVS observed at 137.97 and 129.20 ppm corresponding to Si–CH=CH<sub>2</sub> and Si–CH=CH<sub>2</sub> units also disappeared, while the aliphatic carbons were still present at ca. 57.57–65.65 ppm in  $^{13}\text{C}$  solid-state NMR spectra (Fig. 4(b)) after hydrosilylation to form OVS-DDSQ hybrid. Furthermore, the  $^{29}\text{Si}$  NMR analysis of OVS displayed a single signal of Si–O–Si unit at –80.65 ppm due to its symmetric structure as displayed in Fig. 4(c). After hydrosilylation to form OVS-POSS hybrid, the signals were observed at –21.22, –65.98, and –78.71 ppm in the  $^{29}\text{Si}$  solid-state NMR analyses, which are ascribed to the Si–CH, Si–O–Si ( $T_2$ ) and Si–O–Si ( $T_3$ ) units in the hybrid framework. According to these spectral analyses conducted previously provided the confirmation of the successful synthesis of the OVS-DDSQ hybrid framework. Furthermore, Fig. 4(d) presents the corresponding TGA analyses of DDSQ, OVS, and OVS-DDSQ hybrid where OVS only exhibited  $T_{d10}$  = 247 °C, and char yield = 3.4 wt%. In contrast, the rigid OVS-DDSQ hybrid framework displayed the highest thermal stability of  $T_{d10}$  = 596 °C, and char yield = 82.2 wt%.

Fig. 5 summarizes the TGA results of DVB-DDSQ, DVDDSQ-DDSQ, and OVS-DDSQ hybrids, where  $T_{d10}$  values are 558, 573, and 596 °C, and char yields are 74.0, 79.2, and 82.2 wt%, respectively. Comparatively, the DVB-DDSQ hybrid possesses the lowest thermal stability since the benzene unit is susceptible to pyrolysis compared to the DDSQ and

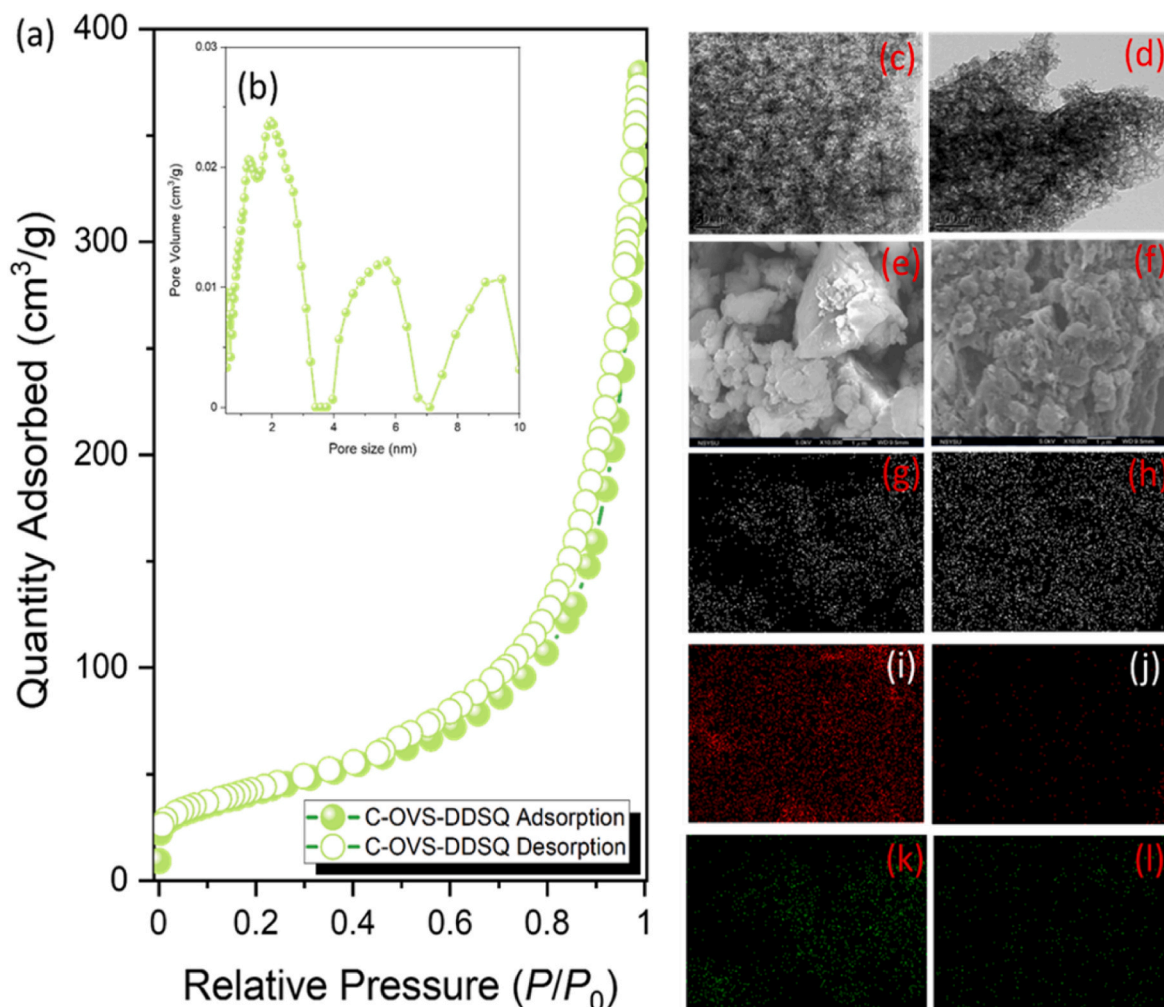
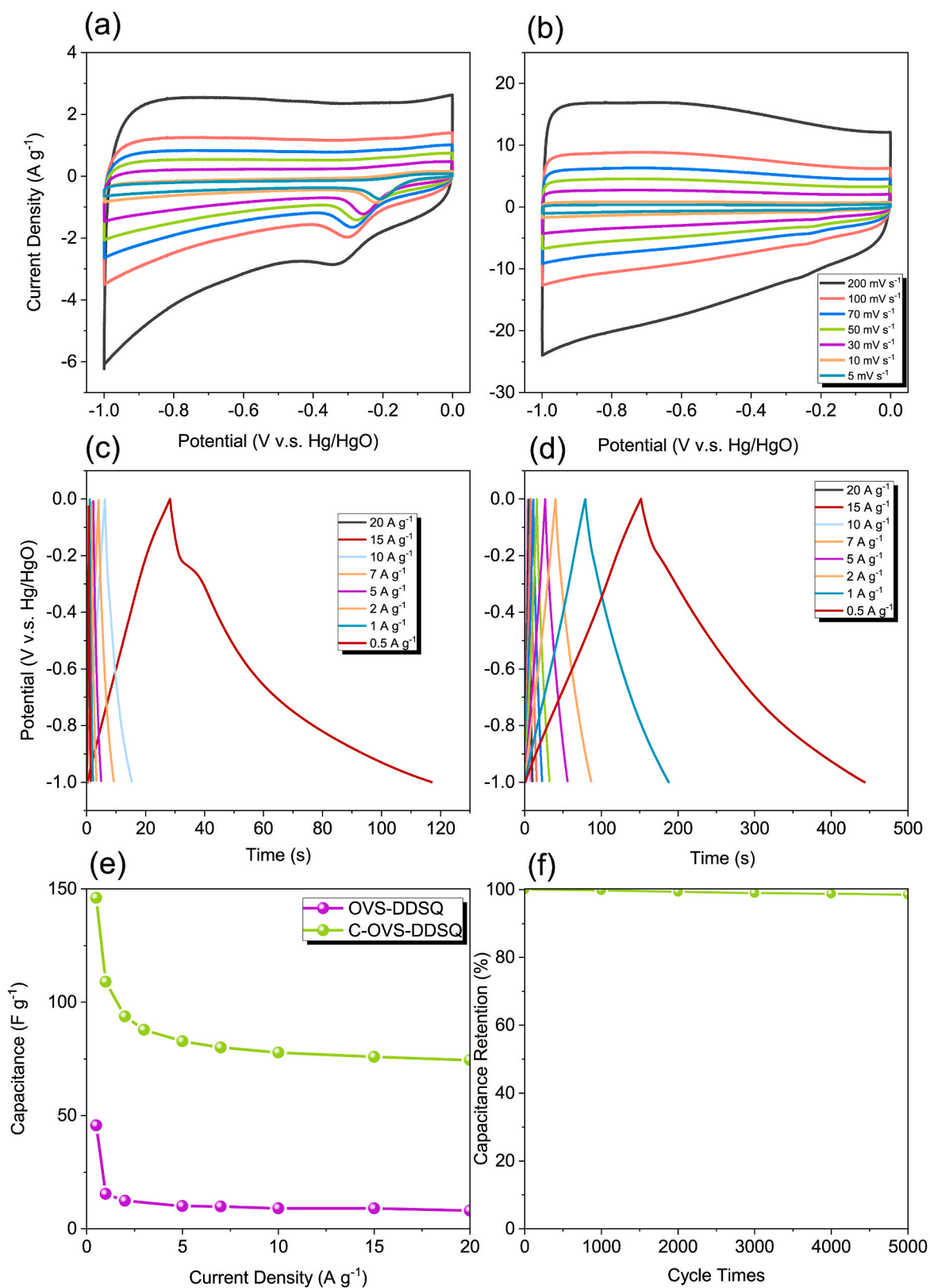


Fig. 6. (A)  $\text{N}_2$  adsorption/desorption isotherms (b) pore size patterns of the C-OVS-DDSQ hybrid and (c–d) TEM (e–f) SEM (g–h) C-, (i–j) Si-, (k–l) O-, and mappings of OVS-DDSQ (c, e, g, i, and k) and C-OVS-DDSQ (d, f, h, j, l). The scale bar in TEM and SEM images was 20 nm and 1  $\mu\text{m}$ : respectively.



**Fig. 7.** (A–b) CV, (c–d) GCD curves of OVS-DDSQ (a, c) and C-OVS-DDSQ hybrid (b, d), (e) capacitance performance of OVS-DQ and C-OVS-DDSQ, and (f) capacitance retention of C-OVS-DDSQ hybrid framework.

OVS units. In addition, the OVS-DDSQ hybrid, which incorporates two types of POSS nanoparticles and utilizes an octa-functionalized group, shows the highest thermal stability as expected. This result could be attributed to the enhanced cross-linking structure and increased density within the OVS-DDSQ hybrid.

### 3.4. The preparation of porous carbon from OVS-DDSQ by carbonization

Indeed, the OVS-DDSQ hybrid, with its crosslinking structure with porous property, may have the potential application in electrochemical tests. Furthermore, the OVS-DDSQ hybrid has the advantage of its high thermal stability, which makes its structure not easy to collapse and remains intact even at high temperatures. This characteristic opens up the increase of its specific surface area through carbonization in order to improve its electrochemical performance. We can expect that the organic components could be removed by subjecting the OVS-DDSQ hybrid to carbonization and then forming a C-OVS-DDSQ hybrid framework, leaving behind a carbonaceous framework [41,42]. This carbonized structure usually could provide a high surface area, which is beneficial for electrochemical application since a high surface area allows for better accessibility of the active site and enhances the charge transfer kinetics, ultimately improving the electrochemical performance of this hybrid [91,92]. The XPS analysis of the porous C-OVS-DDSQ hybrid framework [Fig. S4] revealed prominent peaks at specific binding energies: 103.5 eV for Si2p, 284.21 eV for C1s, and 532.09 eV for O1s. Furthermore, XRD analysis, as shown in Fig. S5, revealed that the porous C-OVS-DDSQ hybrid framework displayed two prominent peaks at 20.7° and 37°, which can be attributed to the (002) and (101) diffractions of graphitic crystalline structures, respectively. The porosity properties of the porous C-OVS-DDSQ hybrid framework were confirmed by N<sub>2</sub> adsorption-desorption isothermal analyses at 77 K and 1 bar as displayed in Fig. 6. The C-OVS-DDSQ hybrid exhibited the type II isotherms based on the IUPAC classification. It has a sharp N<sub>2</sub> uptake at both low and high relative pressure ( $P/P_0$ ), corresponding to the presence of both micropore and mesopore characteristics. In Fig. 6(a)–(b), the C-OVS-DDSQ hybrid framework provides a  $S_{\text{BET}}$  surface area of 169 m<sup>2</sup> g<sup>-1</sup> and the pore size diameters based on nonlocal density functional theory (NL-DFT) were ca. 2.2 and 5.4 nm, respectively. The morphology of OVS-DDSQ and C-OVS-DDSQ hybrids was confirmed by FE-SEM and HR-TEM as shown in Fig. 6(c)–6(f). The SEM image of OVS-DDSQ exhibited small spheres with a lumpy and irregular structure (Fig. 6(c)) and the TEM image also showed the absence of long-range ordering of this hybrid (Fig. 6(e)). After carbonization to form the C-OVS-DDSQ hybrid, the SEM image shows the lump structure and transforms into smaller lumps (Fig. 6(f)) and the TEM image also displays the porous nature character (Fig. 6(d)). In addition, the carbon content was significantly increased after carbonization based on EDX analyses as shown in Fig. 6(g)–6(j) and summarized in Table S1, indicating the carbonaceous framework was obtained after removing the organic component.

The electrochemical performance of OVS-DDSQ and porous C-OVS-DDSQ hybrid frameworks were estimated through cyclic voltammetry (CV) and galvanostatic charge-discharge (GCD) analyses in 1 M KOH aqueous solution using the three-electrode system. The CV curves were determined at various scan rates of 5–200 mV s<sup>-1</sup> within the potential window from 0 to -1 V (vs. Hg/HgO) as displayed in Fig. 7(a)–(b). The CV curves of the OVS-DDSQ hybrid (Fig. 7(a)) exhibited rectangular-like shapes with humps, indicating a capacitive response originating from EDLC, which is relatively small. The humps in the rectangular-like shape present the capacitive response of pseudocapacitance and it is attributed to the electron-rich phenyl rings in the structure.

After the carbonization, the C-OVS-DDSQ hybrid provides a much higher area for the EDLC at all the tested scan rates (Fig. 7(b)). The enhanced performance of EDLC is attributed to the higher surface area for electron transfer and the presence of more active sites on the electrode surface from material after carbonization. Fig. 6(c) and (d) show

the GCD curves of OVS-DDSQ and C-OVS-DDSQ hybrids, recorded at different current densities. Both OVS-DDSQ and C-OVS-DDSQ hybrids provided the capacitances of 45.66 F g<sup>-1</sup> and 146 F g<sup>-1</sup> at 0.5 A g<sup>-1</sup> in Fig. 6(e). Moreover, the curves of these two samples were triangular in shape with a slight bend, suggesting both EDLC and pseudocapacity characteristics. The capacitance of the C-OVS-DDSQ hybrid framework is higher than that of OVS-DDSQ primarily due to the presence of carbon in the hybrid structure. The incorporation of carbon-based materials introduces additional charge storage sites and enhances the overall capacitance of the framework. This increased capacitance is attributed to the unique properties of porous carbon, such as its high surface area, conductivity, and ability to form double-layer capacitors. Consequently, the C-OVS-DDSQ hybrid framework offers improved capacitance performance compared to the OVS-DDSQ framework. Finally, the capacitance retention of the C-OVS-DDSQ hybrid shows a high stability of 98.5 % after 5000 cycles (Fig. 6(f)); however, the OVS-DDSQ hybrid did not display any stability in this particular measurement. Overall, the carbonization of the OVS-DDSQ hybrid demonstrates higher electrochemical performance, increasing capacitance and enhanced stability, and a large area for EDLC.

## 4. Conclusions

Three different types of organic-inorganic hybrids of DVB-DDSQ, DVDDSQ-DDSQ, and OVS-DDSQ were synthesized simultaneously by using DDSQ to connect with DVB, DV-DDSQ, and OVS. Both main chain types of DVB-DDSQ and DVDDSQ-DDSQ display high  $T_g$  values (260 and 355 °C),  $T_{d10}$  value at 550 °C, and char yield upon 74 wt%. To further increase the thermal stability, the OVS was incorporated into the DDSQ to form a crosslinked structure of OVS-DDSQ hybrid framework also through hydrosilylation, which displayed the highest thermal stability ( $T_{d10}$  = 596 °C and char yield = 82.2 wt%). This result could be attributed to the enhanced cross-linking structure and increased density within the OVS-DDSQ hybrid. The carbonization of the OVS-DDSQ hybrid to form the C-OVS-DDSQ hybrid demonstrates the higher electrochemical capacitances of 146 F g<sup>-1</sup> at 0.5 A g<sup>-1</sup> and shows the capacitance retention with the high stability of 98.5 % after 5000 cycles because of its high surface area of 169 m<sup>2</sup> g<sup>-1</sup> for electron transfer and the presence of more active sites on the electrode surface from the material.

## 5. CRediT authorship contribution statement

Cheng-Yu Chen: Investigation, Methodology, Writing—original draft. Mohamed Gamal Mohamed: Investigation, Methodology, Conceptualization, Supervision, Writing – original draft. Wei-Cheng Chen: Investigation, Methodology, Writing – original draft. Shiao-Wei Kuo: Supervision.

## Declaration of competing interest

The authors declare that they have no known competing financial interests or personal relationships that could have appeared to influence the work reported in this paper.

## Data availability

The data that has been used is confidential.

## Acknowledgments

This study was supported financially by the Ministry of Science and Technology, Taiwan, under contracts NSTC 110-2124-M-002-013, NSTC 111-2223-E-110-004, NSTC 111-2628-E-007-009, NSTC 111-2221-E-007 -004 and NSTC 111-2622-8-007-011. The authors thank the staff at National Sun Yat-sen University for their assistance with the TEM (ID: EM022600) experiments.

## Appendix A. Supplementary data

Supplementary data to this article can be found online at <https://doi.org/10.1016/j.mtchem.2023.101773>.

## References

- [1] S.W. Kuo, F.C. Chang, POSS related polymer nanocomposites, *Prog. Polym. Sci.* 36 (2011) 1649–1696, <https://doi.org/10.1016/j.progpolymsci.2011.05.002>.
- [2] W.C. Zhang, G. Camino, R. Yang, Polymer/polyhedral oligomeric silsesquioxane (POSS) nanocomposites: an overview of fire retardance, *Prog. Polym. Sci.* 67 (2017) 77–125, <https://doi.org/10.1016/j.progpolymsci.2016.09.011>.
- [3] W.W. Young, J.P. Saez, R. Katsumata, Rationalizing the composition dependence of glass transition temperatures in amorphous polymer/POSS composites, *ACS Macro Lett.* 10 (2021) 1404–1409, <https://doi.org/10.1021/acsmacrolett.1c00597>.
- [4] W.W. Young, R. Shi, X.M. Jia, H.J. Qian, R. Katsumata, Relating the degree of nanofiller functionality to the glass transition temperature and structure in a polymer–polyhedral oligomeric silsesquioxane nanocomposite, *Macromolecules* 55 (2022) 489–4898, <https://doi.org/10.1021/acs.macromol.2c00646>.
- [5] M.G. Mohamed, S.W. Kuo, Functional silica and carbon nanocomposites based on polybenzoxazines, *Macromol. Chem. Phys.* 220 (2019), 1800306, <https://doi.org/10.1002/macp.201800306>.
- [6] S.W. Kuo, Hydrogen bonding interactions in polymer/polyhedral oligomeric silsesquioxane nanomaterials, *J. Polym. Res.* 29 (2022) 69, <https://doi.org/10.1007/s10965-021-02885-4>.
- [7] M.G. Mohamed, S.W. Kuo, Progress in the self-assembly of organic/inorganic polyhedral oligomeric silsesquioxane (POSS) hybrids, *Soft Matter* 18 (2022) 5535–5561, <https://doi.org/10.1039/D2SM00635A>.
- [8] X. Zhang, W. Wei, X. Jin, H. Xiong, Chain dimension and dynamics of polymers in well-defined non-sticky nanocomposites of molecular nanoparticle polyhedral oligomeric silsesquioxane/poly (butylene oxide), *Macromolecules* 53 (2020) 5627–5637, <https://doi.org/10.1021/acs.macromol.0c00158>.
- [9] H. Yang, C. He, T.P. Russell, D. Wang, Epoxy-polyhedral oligomeric silsesquioxanes (POSS) nanocomposite vitrimers with high strength, toughness, and efficient relaxation, *Giant* 4 (2020), 100035, <https://doi.org/10.1016/j.giant.2020.100035>.
- [10] H. Hou, J. Li, X. Li, J. Forth, J. Yin, X. Jiang, B.A. Helms, T.P. Russell, Interfacial activity of amine-functionalized polyhedral oligomeric silsesquioxane (POSS): a simple strategy to structure liquids, *Angew. Chem. Int. Ed.* 131 (2019) 10248–10253, <https://doi.org/10.1002/ange.201903420>.
- [11] H. Wang, G. Hang, H. Mei, L. Li, S. Zheng, Crosslinking of poly(n-butyl acrylate)-POSS copolymers via dynamic urea exchange enables self-healing, reprocessing and shape recovery, *Polym. Chem.* 14 (2023) 872–887, <https://doi.org/10.1039/D2PY01414A>.
- [12] C.W. Chiou, Y.C. Lin, L. Wang, R. Maeda, T. Hayakawa, S.W. Kuo, Hydrogen bond interactions mediate hierarchical self-assembly of POSS-containing block copolymers blended with phenolic resin, *Macromolecules* 47 (2014) 8709–8721, <https://doi.org/10.1021/ma502180c>.
- [13] W.H. Hu, K.W. Huang, C.W. Chiou, S.W. Kuo, Complementary multiple hydrogen bonding interactions induce the self-assembly of supramolecular structures from heteronucleobase-functionalized benzoxazine and polyhedral oligomeric silsesquioxane nanoparticles, *Macromolecules* 45 (2012) 9020–9028, <https://doi.org/10.1021/ma302077x>.
- [14] L. Jin, C. Hong, X. Li, Z. Sun, F. Feng, H. Liu, Corner-opening and corner-capping of mono-substituted T8 POSS: product distribution and isomerization, *Chem. Commun.* 58 (2022) 1573–1576, <https://doi.org/10.1039/D1CC06258A>.
- [15] W. Li, H. Liu, Novel organic–inorganic hybrid polymer based on fluorinated polyhedral oligomeric silsesquioxanes for stable superamphiphobic fabrics and aluminum corrosion protection, *Mater. Today Chem.* 29 (2023), 101390, <https://doi.org/10.1016/j.mtchem.2023.101390>.
- [16] J. Wang, D.L. Zhou, X. Lin, J.H. Li, D. Han, H. Bai, Q. Fu, Preparation of Low-k Poly (dicyclopentadiene) nanocomposites with excellent comprehensive properties by adding larger POSS, *Chem. Eng. J.* 439 (2022), 135737, <https://doi.org/10.1016/j.cej.2022.135737>.
- [17] Y.C. Huang, W.C. Chen, S.W. Kuo, Mesoporous phenolic/POSS hybrids induced by microphase separation arising from competitive hydrogen bonding interactions, *Macromolecules* 55 (2022) 8918–8930, <https://doi.org/10.1021/acs.macromol.2c01585>.
- [18] W.C. Chen, Y.T. Liu, S.W. Kuo, Highly thermal stable phenolic resin based on double-decker-shaped POSS nanocomposites for supercapacitors, *Polymers* 12 (2020) 2151, <https://doi.org/10.3390/polym12092151>.
- [19] S. Shi, X. Liao, W. Tang, P. Song, F. Zhou, Z. Fan, F. Guo, G. Li, Ultralow dielectric constant polyarylene ether nitrile/polyhedral oligomeric silsesquioxanes foams with high thermal stabilities and excellent mechanical properties prepared by supercritical CO<sub>2</sub>, *Adv. Eng. Mater.* 24 (2022), 2100874, <https://doi.org/10.1002/adem.202100874>.
- [20] S. Teng, Z. Jiang, Z. Qiu, Effect of different POSS structures on the crystallization behavior and dynamic mechanical properties of biodegradable Poly (ethylene succinate), *Polymer* 163 (2019) 68–73, <https://doi.org/10.1016/j.polymer.2018.12.061>.
- [21] A. Romo-Urbe, J.D. Lichtenhan, Melt extrusion and blow molding parts-per-million POSS interspersed the macromolecular network and simultaneously enhanced thermomechanical and barrier properties of polyolefin films, *Polym. Eng. Sci.* 61 (2021) 245–257, <https://doi.org/10.1002/pen.25572>.
- [22] X. Ye, X. Meng, Z. Han, Y. Qi, Z. Li, P. Tian, W. Wang, J. Li, Y. Li, W. Zhang, R. Yang, Designing Fe-containing polyhedral oligomeric silsesquioxane to endow superior mechanical and flame-retardant performances of polyamide 1010, *Compos. Sci. Technol.* 233 (2023), 109894, <https://doi.org/10.1016/j.compscitech.2022.109894>.
- [23] H. Wu, B. Zeng, J. Chen, T. Wu, Y. Li, Y. Liu, L. Dai, An intramolecular hybrid of metal polyhedral oligomeric silsesquioxanes with special titanium-embedded cage structure and flame retardant functionality, *Chem. Eng. J.* 374 (2019) 1304–1316, <https://doi.org/10.1016/j.cej.2019.06.027>.
- [24] T.C. Chou, W.C. Chen, M.G. Mohamed, Y.C. Huang, S.W. Kuo, Organic-inorganic phenolic/POSS hybrids provide highly ordered mesoporous structures templated by high thermal stability of PS-b-P4VP diblock copolymer, *Chem. Eur. J.* 29 (2023), e202300538, <https://doi.org/10.1002/chem.202300538>.
- [25] Y. Liu, X.Y. Yan, Q.Y. Guo, H. Lei, X.Y. Liu, X.H. Li, Y. Wu, W. Zhang, G.X. Liu, S.Z. D. Cheng, Recent progress on the rheology of giant molecules, *Macromol. Chem. Phys.* 224 (2023), 2200357, <https://doi.org/10.1002/macp.202200357>.
- [26] E. Szefer, K. Stafin, A. Leszczynska, P. Zajac, E. Hebda, K.N. Raftopoulos, K. Pieliowski, Morphology, dynamics, and order development in a thermoplastic polyurethane with melt blended POSS, *J. Polym. Sci., Part B: Polym. Phys.* 57 (2019) 1133–1142, <https://doi.org/10.1002/polb.24868>.
- [27] S.W. Kuo, H.C. Lin, W.J. Huang, C.F. Huang, C.F. Chang, Hydrogen bonding interactions and miscibility between phenolic resin and octa(acetoxystyryl) polyhedral oligomeric silsesquioxane (AS-POSS) nanocomposites, *J. Polym. Sci., Part B: Polym. Phys.* 44 (2006) 673–686, <https://doi.org/10.1002/polb.20731>.
- [28] S. Liu, R. Guo, C. Li, C. Lu, G. Yang, F. Wang, J. Lie, C. Ma, M. Gao, POSS hybrid hydrogels: a brief review of synthesis, properties and applications, *Eur. Polym. J.* 143 (2021), 110180, <https://doi.org/10.1016/j.eurpolymj.2020.110180>.
- [29] I. Lin, C.C. Hsu, T.C. Yu, S.W. Kuo, W.T. Chuang, Y.W. Chiang, Propagatable hierarchical architectures from dispersive fragments to periodic nanosheets within phase-separated nanostructures by controlling guest–host interaction, *Macromolecules* 55 (2022) 9048–9056, <https://doi.org/10.1021/acs.macromol.2c01643>.
- [30] Q.Y. Guo, X.Y. Yan, W. Zhang, X.H. Li, Y. Xu, S. Dai, Y. Liu, B.X. Zhang, X. Feng, J. Yin, D. Han, J. Huang, Z. Su, T. Liu, M. Huang, C.H. Hsu, S.Z.D. Cheng, Ordered mesoporous silica pyrolyzed from single-source self-assembled organic–inorganic giant surfactants, *J. Am. Chem. Soc.* 143 (2021) 12935–12942, <https://doi.org/10.1021/jacs.1c05356>.
- [31] M.G. Mohamed, S.W. Kuo, Polybenzoxazine/polyhedral oligomeric silsesquioxane (POSS) nanocomposites, *Polymers* 8 (2016) 225, <https://doi.org/10.3390/polym8060225>.
- [32] H. Berk, M. Kaya, A. Cihaner, Thermally highly stable polyhedral oligomeric silsesquioxane (POSS)-sulfur based hybrid inorganic/organic polymers: synthesis, characterization and removal of mercury ion, *Polym. Chem.* 13 (2022) 5152–5158, <https://doi.org/10.1039/D2PY00761D>.
- [33] M.G. Mohamed, M.Y. Tsai, C.F. Wang, C.F. Huang, M. Danko, L. Dai, L. Chen, S. W. Kuo, Multifunctional polyhedral oligomeric silsesquioxane (POSS) based hybrid porous materials for CO<sub>2</sub> uptake and iodine adsorption, *Polymers* 13 (2021) 221, <https://doi.org/10.3390/polym13020221>.
- [34] M.G. Mohamed, M.H. Elsayed, Y. Ye, M.M. Samy, A.E. Hassan, T.H. Mansoure, Z. Wen, H.H. Chou, K.H. Chen, S.W. Kuo, Construction of porous organic/inorganic hybrid polymers based on polyhedral oligomeric silsesquioxane for energy storage and hydrogen production from water, *Polymers* 15 (2023) 182, <https://doi.org/10.3390/polym15010182>.
- [35] M. Ejaz, M.M. Samy, Y. Ye, S.W. Kuo, M.G. Mohamed, Design hybrid porous organic/inorganic polymers containing polyhedral oligomeric silsesquioxane/pyrene/anthracene moieties as a high-performance electrode for supercapacitor, *Int. J. Mol. Sci.* 24 (2023) 2501, <https://doi.org/10.3390/ijms24032501>.
- [36] S. Wu, T. Hayakawa, M. Kakimoto, H. Oikawa, Synthesis and characterization of organosoluble aromatic polyimides containing POSS in main chain derived from double-decker-shaped silsesquioxane, *Macromolecules* 41 (2008) 3481–3487, <https://doi.org/10.1021/ma7027227>.
- [37] M.G. Mohamed, S.W. Kuo, Functional polyimide/polyhedral oligomeric silsesquioxane nanocomposites, *Polymers* 11 (2019) 26, <https://doi.org/10.3390/polym11010026>.
- [38] C.H. Chiang, M.G. Mohamed, W.C. Chen, M. Madhu, W.L. Tseng, S.W. Kuo, Construction of fluorescent conjugated polytriazole containing double-decker silsesquioxane: click polymerization and thermal stability, *Polymers* 15 (2023) 331.
- [39] Y.T. Liao, Y.C. Lin, S.W. Kuo, Highly thermally stable, transparent, and flexible polybenzoxazine nanocomposites by combination of double-decker-shaped polyhedral silsesquioxanes and polydimethylsiloxane, *Macromolecules* 50 (2017) 5739–5747, <https://doi.org/10.1021/acs.macromol.7b01085>.
- [40] X. Lin, X. Deng, Y.Y. Zhang, Q. Zhang, H. Di, Q. Fu, Effect of POSS size on the porosity and adsorption performance of hybrid porous polymers, *Macromolecules* 56 (2023) 1243–1252, <https://doi.org/10.1021/acs.macromol.2c02486>.
- [41] M.G. Mohamed, W.C. Chen, A.F.M. El-Mahdy, S.W. Kuo, Porous organic/inorganic polymers based on double-decker silsesquioxane for high-performance energy

- storage, *J. Polym. Res.* 28 (2021) 219, <https://doi.org/10.1007/s10965-021-02579-x>.
- [42] M.G. Mohamed, T.H. Mansoure, Y. Takashi, M.M. Samy, T. Chen, S.W. Kuo, Ultrastable porous organic/inorganic polymers based on polyhedral oligomeric silsesquioxane (POSS) hybrids exhibiting high performance for thermal property and energy storage, *Microporous Mesoporous Mater.* 328 (2021), 111505, <https://doi.org/10.1016/j.micromeso.2021.111505>.
- [43] X. Zhao, Q. Wang, R. Kunthom, H. Liu, Sulfonic acid-grafted hybrid porous polymer based on double-decker silsesquioxane as highly efficient acidic heterogeneous catalysts for the alcoholysis of styrene oxide, *ACS Appl. Mater. Interfaces* 15 (2023) 6657–6665, <https://doi.org/10.1021/acsami.2c17732>.
- [44] M.G. Mohamed, S.U. Sharma, C.H. Yang, M.M. Samy, A.A.K. Mohammed, S. V. Chaganti, J.T. Lee, S.W. Kuo, Anthraquinone-enriched conjugated microporous polymers as organic cathode materials for high-performance lithium-ion batteries, *ACS Appl. Energy Mater.* 4 (2021) 14628–14639, <https://doi.org/10.1021/acsaem.1c03270>.
- [45] P.N. Singh, M.G. Mohamed, S.V. Chaganti, S.U. Sharma, M. Ejaz, J.T. Lee, S. W. Kuo, Rational design of ultrastable conjugated microporous polymers based on pyrene and perylene units as high-performance organic electrode materials for supercapacitor applications, *ACS Appl. Energy Mater.* 6 (2023) 8277–8287, <https://doi.org/10.1021/acsaem.3c01391>.
- [46] T.H. Weng, M.G. Mohamed, S.U. Sharma, S.V. Chaganti, M.M. Samy, J.T. Lee, S. W. Kuo, Ultrastable three-dimensional triptycene- and tetraphenylethene-conjugated microporous polymers for energy storage, *ACS Appl. Energy Mater.* 5 (2022) 14239–14249.
- [47] M.G. Mohamed, S.V. Chaganti, S.U. Sharma, M.M. Samy, M. Ejaz, J.T. Lee, K. Zhang, S.W. Kuo, Constructing conjugated microporous polymers containing the pyrene-4,5,9,10-tetraone unit for energy storage, *ACS Appl. Energy Mater.* 5 (2022) 10130–10140, <https://doi.org/10.1021/acsaem.2c01842>.
- [48] M.G. Mohamed, M.M. Samy, T.H. Mansoure, S.U. Sharma, M.S. Tsai, J.H. Chen, J. T. Lee, S.W. Kuo, Dispersions of 1,3,4-oxadiazole-linked conjugated microporous polymers with carbon nanotubes as a high-performance electrode for supercapacitors, *ACS Appl. Energy Mater.* 5 (2022) 3677–3688.
- [49] M. Inagaki, Q. Konno, O. Tanaike, Carbon materials for electrochemical capacitors, *J. Power Sources* 195 (2020) 7880–7903, <https://doi.org/10.1016/j.jpowsour.2010.06.036>.
- [50] M.G. Mohamed, S.V. Chaganti, M.S. Li, M.M. Samy, S.U. Sharma, J.T. Lee, M. H. Elsayed, H.H. Chou, S.W. Kuo, Ultrastable porous organic polymers containing thianthrene and pyrene units as organic electrode materials for supercapacitors, *ACS Appl. Energy Mater.* 5 (2022) 6442–6452.
- [51] M.G. Mohamed, S.Y. Chang, M. Ejaz, M.M. Samy, A.O. Mousa, S.W. Kuo, Design and synthesis of bisulfone-linked two-dimensional conjugated microporous polymers for CO<sub>2</sub> adsorption and energy storage, *Molecules* 28 (2023) 3234.
- [52] X. Dong, H. Jin, R. Wang, J. Zhang, X. Feng, C. Yan, S. Chen, S. Wang, J. Wang, J. Lu, High volumetric capacitance, ultralong life supercapacitors enabled by waxberry-derived hierarchical porous carbon materials, *Adv. Energy Mater.* 8 (2018), 1702695, <https://doi.org/10.1002/aenm.201702695>.
- [53] S.Y. Chang, A.M. Elewa, M.G. Mohamed, I.M.A. Mekhemer, M.M. Samy, K. Zhang, H.H. Chou, S.W. Kuo, Rational design and synthesis of bifunctional Dibenzof[*g*,*p*]chrysene-based conjugated microporous polymers for energy storage and visible light-driven photocatalytic hydrogen evolution, *Mater. Today Chem.* 33 (2023), 101680.
- [54] M.G. Mohamed, H.Y. Hu, M. Madhu, M.M. Samy, I.M.A. Mekhemer, W.L. Tseng, H. H. Chou, S.W. Kuo, Ultrastable two-dimensional fluorescent conjugated microporous polymers containing pyrene and fluorene units for metal ion sensing and energy storage, *Eur. Polym. J.* 189 (2023), 111980.
- [55] M.G. Mohamed, A.M. Elewa, M.S. Li, S.W. Kuo, Construction and multifunctional of hypercrosslinked porous organic polymers containing ferrocene unit for high-performance iodine adsorption and supercapacitor, *J. Taiwan Inst. Chem. Eng.* 150 (2023), 105045, <https://doi.org/10.1016/j.jtice.2023.105045>.
- [56] X. Guan, Y. Zhao, H. Pei, M. Zhao, Y. Wang, X. Zhou, M.G. Mohamed, S.W. Kuo, Y. Ye, Metalloporphyrin conjugated porous polymer in-situ grown on a Celgard separator as multifunctional polysulfide barrier and catalyst for high-performance Li-S batteries, *Chem. Eng. J.* 473 (2023), 144733.
- [57] A. Dutta, S. Mitra, M. Basak, T. Banerjee, A Comprehensive Review on Batteries and Supercapacitors: Development and Challenges since Their Inception, *Energy Storage*, 2022, p. e339, <https://doi.org/10.1002/est2.339>.
- [58] A.Z. Al Shaqsi, K. Sopian, A. Al-Hinai, Review of energy storage services, applications, limitations, and benefits, *Energy Rep.* 6 (2020) 288–306, <https://doi.org/10.1016/j.egy.2020.07.028>.
- [59] S. Roldán, D. Barreda, M. Granda, M. Menéndez, R. Santamaría, C. Blanco, An approach to classification and capacitance expressions in electrochemical capacitors Technology, *Phys. Chem. Chem. Phys.* 17 (2015) 1084–1092, <https://doi.org/10.1039/c4cp05124f>.
- [60] S. Najib, E. Erdem, Current progress achieved in novel materials for supercapacitor electrodes: mini review, *Nanoscale Adv.* 1 (2019) 2817–2827, <https://doi.org/10.1039/C9NA00345B>.
- [61] G.Z. Chen, Understanding supercapacitors based on nano-hybrid materials with interfacial conjugation, *Prog. Nat. Sci.* 23 (2013) 245–255, <https://doi.org/10.1016/j.pnsc.2013.04.001>.
- [62] S. Fleischmann, J.B. Mitchell, R. Wang, C. Zhan, D.E. Jiang, V. Presse, V. Augustyn, Pseudocapacitance: from fundamental understanding to high power energy storage materials, *Chem. Rev.* 120 (2022) 6738–6782, <https://doi.org/10.1021/acs.chemrev.0c00170>.
- [63] B.E. Conway, V. Birs, J. Wojtowicz, The role and utilization of pseudocapacitance for energy storage by supercapacitors, *J. Power Sources* 66 (1997) 1–14, [https://doi.org/10.1016/S0378-7753\(96\)02474-3](https://doi.org/10.1016/S0378-7753(96)02474-3).
- [64] Y. Liu, S.P. Jiang, Z. Shao, Intercalation pseudocapacitance in electrochemical energy storage: recent advances in fundamental understanding and materials development, *Mater. Today Adv.* 7 (2020), 100072, <https://doi.org/10.1016/j.mtdadv.2020.100072>.
- [65] V. Augustyn, P. Simon, B. Dunn, Pseudocapacitive oxide materials for high-rate electrochemical energy storage, *Energy Environ. Sci.* 7 (2014) 1597–1614, <https://doi.org/10.1039/c3ee44164d>.
- [66] J. Libich, J. Máca, J. Vondrák, O. Čech, Sedlářková, M. Supercapacitors, Properties and applications, *J. Energy Storage* 17 (2018) 224–227, <https://doi.org/10.1016/j.est.2018.03.012>.
- [67] B. Lobato, L. Suárez, L. Guardia, T.A. Centeno, Capacitance and surface of carbons in supercapacitors, *Carbon* 122 (2017) 434–445, <https://doi.org/10.1016/j.carbon.2017.06.083>.
- [68] R. Heimbockel, F. Hoffmann, M. Froba, Insights into the influence of the pore size and surface area of activated carbons on the energy storage of electric double layer capacitors with a new potentially universally applicable capacitor model, *Phys. Chem. Chem. Phys.* 21 (2019) 3122–3133, <https://doi.org/10.1039/C8CP06443A>.
- [69] M. Kim, K.L. Firestein, J.F.S. Fernando, X. Xu, H. Lim, D.V. Golberg, J. Na, i. Kim, H. Nara, J. Tang, Y. Yamauchi, Strategic design of Fe and N co-doped hierarchically porous carbon as superior ORR catalyst: from the perspective of nanoarchitectonics, *Chem. Sci.* 13 (2022) 10836–10845.
- [70] L. Borchardt, Q.L. Zhu, M.E. Casco, R. Berger, X. Zhuang, S. Kaskel, X. Feng, Q. Xu, Toward a molecular design of porous carbon materials, *Mater. Today* 20 (2017) 592–610, <https://doi.org/10.1016/j.mattod.2017.06.002>.
- [71] J. Wang, Y. Wang, H. Hu, Q. Yang, J. Cai, From metal-organic frameworks to porous carbon materials: recent progress and prospects from energy and environmental perspectives, *Nanoscale* 12 (2020) 4238–4268, <https://doi.org/10.1039/C9NR09697C>.
- [72] L. Wang, X. Hu, Recent advances in porous carbon materials for electrochemical energy storage, *Chem. Asian J.* 13 (2018) 1518–1529, <https://doi.org/10.1002/asia.201800553>.
- [73] J. Yin, W. Zhang, N.A. Alhebshi, N. Salah, H.F. Alshareef, Synthesis strategies of porous carbon for supercapacitor applications, *Small Methods* 4 (2020), 1900853, <https://doi.org/10.1002/smt.201900853>.
- [74] W. Park, G. Park, M. Kim, M. Han, J. Jang, Y. Yamauchi, B. Yulianto, P. Krüger, J. Kim, N. Park, H. Lim, Ni-single atom decorated mesoporous carbon electrocatalysts for hydrogen evolution reaction, *Chem. Eng. J.* 486 (2023), 143733.
- [75] M. Kim, R. Xin, J. Earnshaw, J. Tang, J.P. Hill, A. Ashok, A.K. Nanjundan, J. Kim, C. Young, Y. Sugahara, J. Na, Y. Yamauchi, MOF-derived nanoporous carbons with diverse tunable nanoarchitectures, *Nat. Protoc.* 17 (2022) 2990–3027, <https://doi.org/10.1038/s41596-022-00718-2>.
- [76] F. Xu, Z. Tang, S. Huang, L. Chen, Y. Liang, W. Mai, H. Zhong, R. Fu, D. Wu, Facile synthesis of ultrahigh-surface-area hollow carbon nanospheres for enhanced adsorption and energy storage, *Nat. Commun.* 6 (2015) 7221, <https://doi.org/10.1038/ncomms8221>.
- [77] T. Cai, M. Zhou, G. Han, S. Guan, Phenol–formaldehyde carbon with ordered/disordered bimodal mesoporous structure as high-performance electrode materials for supercapacitors, *J. Power Sources* 241 (2013) 6–11, <https://doi.org/10.1016/j.jpowsour.2013.04.112>.
- [78] R. Chakraborty, K. Vilya, M. Pradhan, A.K. Nayak, Recent advancement of biomass-derived porous carbon-based materials for energy and environmental remediation applications, *J. Mater. Chem. A* 10 (2022) 6965–7005, <https://doi.org/10.1039/D1TA10269A>.
- [79] R.W. Fu, Z.H. Li, Y.R. Liang, F. Li, F. Xu, D.C. Wu, Hierarchical porous carbons: design, preparation, and performance in energy storage, *N. Carbon Mater.* 26 (2011) 171–179, [https://doi.org/10.1016/S1872-5805\(11\)60074-7](https://doi.org/10.1016/S1872-5805(11)60074-7).
- [80] H. Zhang, L. Zhang, J. Chen, H. Su, F. Liu, W. Yang, One-step synthesis of hierarchically porous carbons for high-performance electric double layer supercapacitors, *J. Power Sources* 315 (2016) 120–126, <https://doi.org/10.1016/j.jpowsour.2016.03.005>.
- [81] F. Alves, P. Scholder, I. Nischang, Conceptual design of large surface area porous polymeric hybrid media based on polyhedral oligomeric silsesquioxane precursors: preparation, tailoring of porous properties, and internal surface functionalization, *ACS Appl. Mater. Interfaces* 5 (2013) 2517–2526, <https://doi.org/10.1021/am303048y>.
- [82] F. Alves, I. Nischang, Tailor-made hybrid organic–inorganic porous materials based on polyhedral oligomeric silsesquioxanes (POSS) by the step-growth mechanism of thiol-ene “click” chemistry, *Chem. Eur. J.* 19 (2013) 17310–17313, <https://doi.org/10.1002/chem.201303759>.
- [83] X. Lin, Y.Y. Deng, Q. Zhang, D. Han, Q. Fu, Effect of POSS size on the porosity and adsorption performance of hybrid porous polymers, *Macromolecules* 56 (2023) 1243–1252, <https://doi.org/10.1021/acs.macromol.2c02486>.
- [84] M. Kwasny, A. Kowalewska, K. Wodnicka, M. Handke, Mesoporous silica obtained by polycondensation of octahydrodoctasilsesquioxane, *J. Mater. Sci.* 48 (2013) 5188–5195, <https://doi.org/10.1007/s10853-013-7306-9>.

- [85] Z. Li, D. Wu, Y. Liang, R. Fu, K. Matyjaszewski, Synthesis of well-defined microporous carbons by molecular-scale templating with polyhedral oligomeric silsesquioxane moieties, *J. Am. Chem. Soc.* 136 (2014) 4805–4808, <https://doi.org/10.1021/ja412192v>.
- [86] Y. Liu, M. Kigure, K. Koizumi, N. Takeda, M. Unno, A. Ouali, Synthesis of tetrachloro, tetraiodo, and tetraazido double-decker siloxanes, *Inorg. Chem.* 59 (2020) 15478–15486, <https://doi.org/10.1021/acs.inorgchem.0c02515>.
- [87] J. Duszczyk, K. Mitula, M. Rzonsowska, P. Ławniczak, R. Januszewski, B. Szarlan, B. Dudziec, Slick synthetic approach to various fluoroalkyl silsesquioxanes—assessment of their dielectric properties, *Materials* 5 (2022) 8997, <https://doi.org/10.3390/ma15248997>.
- [88] T. Hamada, S. Takase, A. Tanaka, K. Okada, S. Mineoi, A. Uedono, J. Ohshita, Double-decker silsesquioxane-grafted polysilsesquioxane hybrid films as thermal insulation materials, *ACS Appl. Polym. Mater.* 5 (2023) 743–750, <https://doi.org/10.1021/acscpm.2c01743>.
- [89] M.G. Mohamed, K.C. Hsu, J.L. Hong, S.W. Kuo, Unexpected fluorescence from maleimide-containing polyhedral oligomeric silsesquioxanes: nanoparticle and sequence distribution analyses of polystyrene-based alternating copolymers, *Polym. Chem.* 7 (2016) 135–145, <https://doi.org/10.1039/C5PY01537E>.
- [90] Y.C. Lin, S.W. Kuo, Hierarchical self-assembly and secondary structures of linear polypeptides graft onto POSS in the side chain through click chemistry, *Polym. Chem.* 3 (2012) 162, <https://doi.org/10.1039/C1PY00381J>.
- [91] M.G. Mohamed, M.M. Samy, T.H. Mansoure, C.J. Li, W.C. Li, J.H. Chen, K. Zhang, S.W. Kuo, Microporous carbon and carbon/metal composite materials derived from bio-benzoxazine-linked precursor for CO<sub>2</sub> capture and energy storage applications, *Int. J. Mol. Sci.* 23 (2022) 347, <https://doi.org/10.3390/ijms23010347>.
- [92] J.G. Li, Y.F. Ho, M.M.M. Ahmed, H.C. Liang, S.W. Kuo, Mesoporous carbons templated by PEO-PCL block copolymers as electrode materials for supercapacitors, *Chem. Eur J.* 25 (2019) 10456–10463, <https://doi.org/10.1002/chem.201901724>.